

A Soft, Distributed, Digital 3-axis Skin Sensor Employing a Hybrid Permanent-Adjustable Magnetic Field

Alexis Carlos Holgado¹, Javier Alejandro Alvarez Lopez¹, Tito Pradhono Tomo¹,
 Sophon Somlor¹, Shigeki Sugano¹

Abstract—In this letter, we present a new iteration of a prototype sensor module that can be used as a skin sensor for robots. The sensor uses a hybrid arrangement that consists in a small permanent magnet and an electromagnet working together above a 3-axis magnetic sensor. Both layers are separated by a flexible material that provides compliance to the sensor module. The sensitivity of the sensor can be adjusted by changing the flow of current on the electromagnet, while the permanent magnet increases the intensity of the overall magnetic field to optimize the utilization of the bandwidth of the sensor. Each sensor module includes a microcontroller with digital output that offers multimodal and distributed sensing capabilities. Problem areas of the previous version are indicated, the magnet array idea is presented and tested, and finally experiments are performed on different shapes of a flexible material to be used as middle layer.

I. INTRODUCTION

Embodiment has been an extensively discussed and studied topic in robotics[1][2][3]. A key point of the idea is that robots need to have physical extensions to interact with the surrounding world. In particular, tactile sensing plays a critical role in the way a robot interacts with the world [4][5].

In this letter we want to focus on two main areas that still pose challenges for tactile sensors: coverage of extended surfaces and range of sensitivity that the sensors should support (to accept both strong and delicate interactions). The sensor prototype presented in this work aims to cover these difficulties. The idea behind our sensor is a modular design that allows several units to be interconnected, providing larger sense of touch areas on robots, while also allowing the sensitivity to be adjusted on each module separately. The sensor network is designed to be able to be completely covered by a continuous thin layer of soft material (no holes) and sense 3-axis interaction throughout the covered area.

In a previous paper [6], we presented the first version of the sensor module, that hereafter will be referred to as 'PV'. In the current letter, we offer a new version of the module with several enhancements, that will be called 'NV'.

The operating principle of the PV was: a magnetic field is induced on a flat coil embedded in a printed circuit board (PCB). Then, due to external forces, the position of the field changes over time and a geo-magnetic sensor registers and reports those changes. During past experiments on the PV, we detected that the strength of the magnetic field generated

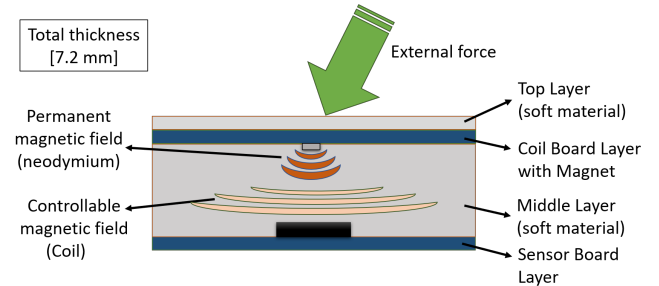


Fig. 1: Layers of sensor module

by the coil did not utilize much of the available bandwidth of the magnetic sensor.

Therefore, the main contribution of this paper is to offer a solution for that problem, along with experimentation on three different shapes for the middle layer that separates the sensor active layers.

The rest of the paper offers the following sections. Section II presents some related works. Section III describes the general operating principle of the sensor, some specifications on each component layer and limitations of the PV that motivated this work. In section IV, we offer solutions for the limitations of the sensor coil board discussed in the previous section, as well as experiments with three different types of permanent magnets. Section V presents experiments with three different shapes of flexible material to be used between the sensor layers. Lastly, Section VI presents conclusions and planned future work.

II. RELATED WORKS

Our sensor module uses a compact integrated system on chip that includes a microcontroller and a 3-axis Hall effect sensor in a single chip. Hall sensors have been reduced in size in recent years, and are now widely used for tactile sensing applications like [7] (also developed in our laboratory). This idea employs a small permanent magnet inside a silicone cover. The spatial resolution is high but the magnetic field intensity cannot be changed dynamically, so the sensitivity range is fixed. Similarly, [8] employs several small magnets in a slightly bigger configuration. The ability for a sensor to cover big areas has been addressed in the comprehensive way on [9]. The designed modules can be interconnected and feature high robustness against problems in the network. However, only normal force can be measured and require small holes on the cover to operate

¹ The authors are with Faculty of Science and Engineering, Modern Mechanical Engineering, Waseda University, Tokyo, Japan. contact: aholgado@fuji.waseda.jp

the optical proximity sensors. The work in [10] utilizes a planar coil similar to our idea; however, once again the sensor measures only one axis and does not implement adjustable sensitivity. Usually sensors are designed and manufactured to operate with a certain sensitivity, with tailored pre-set task requirements, and cannot be changed after production. We argue that the ability of our sensor to measure 3-axis while also having the possibility to adjust its sensitivity represents a strong advantage point.

III. SENSOR MODULE DESCRIPTION

The general working principle of the prototype relies on sensing induced magnetic fields that change position over time due to contact with external forces. The sensor module contains the following layers:

- 1) Sensor Board Layer: The bottom layer of the module, called 'Sensor Board', contains all the sensing electronics.
- 2) Middle Material Layer: A soft deformable material placed between the Sensor Board and the Coil Board.
- 3) Coil Board Layer: The top layer of the sensor, in contact with external forces. It is suspended on top of the Sensor Board, and we call it 'Coil Board'.

A diagram of a sensor module with all the layers can be found in Fig. 1. Strong double-sided sticky tape from Nichiban is used to fix all layers together. Furthermore, a side-by-side comparison between PV and NV can be found in Fig. 2. Further details, problematic areas and suggested solutions for each layer are explained in the next subsections.

A. Sensor Board

The main component of the Sensor Board PCB is a system on chip model BMF055 from Bosch. Containing an ATSAMD20J18 microcontroller and a 9-axis inertial measurement unit that includes a geo-magnetic sensor¹, measures changes in the position (3 axes) of the magnetic field generated by the Coil Board. The BFM055 chip also offers the possibility to process signals locally and control connections with other modules. However, these features are beyond the scope of this paper and will be revisited in the future. Another advantage of the chip is that it provides digital output, with added robustness against electromagnetic noise. The NV of the Sensor Board is very similar to the one presented in [6]; with the only main difference being that flat cable connectors were added to the three communication ports.

B. Middle Material

The PV used a 3mm thick open-cell polymer foam as middle layer. However, it was found to collapse close to its mechanical deformation limit under relatively small normal forces (between 2 and 3N). Shear force tolerance was also small, accepting values below 1N and displacements of less than 1mm, before reaching its breaking point. For the NV,

¹Components inside the chip are: one BMA160 accelerometer, one BMG160 gyroscope and one BMM150 geo-magnetic sensor. The manufacturer of all components is Bosch.

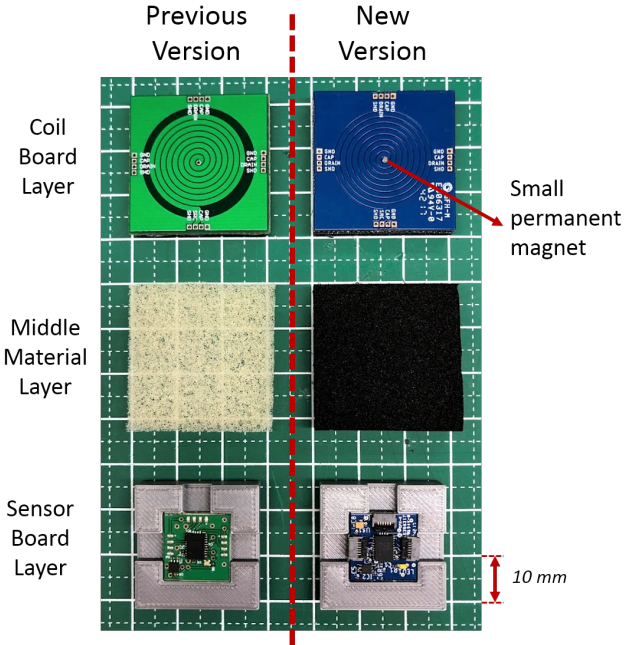


Fig. 2: Previous Version and New Version side by side. All sensor module layers are exposed (prior to assembly)

we decided to use neoprene of 5mm thickness (from Matec Sozai) as deformable material. Preliminary results showed that neoprene can endure higher normal and shear forces (up to ranges of 50N and 10N for normal and shear forces respectively). Three possible shapes of neoprene material are proposed, tested and discussed in Section V.

C. Coil Board

The PV used an embedded flat coil with an outer diameter of 20mm that span over two layers of a PCB, with a resistance of 0.69Ω. Powered with a direct current of 1500mA, the PV coil generated 0.25mT at a distance of 1mm from its surface. In [6], it was discovered that it would be beneficial to have a stronger magnetic field, so the NV was manufactured with a coil of the same outer diameter but thicker copper traces. As a result, the new coil has a resistance of 0.318Ω; thus the magnetic field is nearly 43% stronger than the PV. The NV coil generates a magnetic field of 0.6mT at the same current and distance (1500mA and 1mm).

In previous works, it was detected that applying a current of 1500mA into the coil raised its temperature to a stable 45°C. This temperature has been set as a design limit for our project, based on normal commercial temperature ratings for circuits (0°C-70°C). Therefore, 1500mA has been adopted as the maximum value to be applied on the Coil Board.

Even after the coil design improvements, the new magnetic field was found to be using close to 25% of the Z-axis measurable bandwidth of the sensor (saturation at 2.5mT). A possible solution to better benefit from the bandwidth of the sensor is presented in the subsequent section.

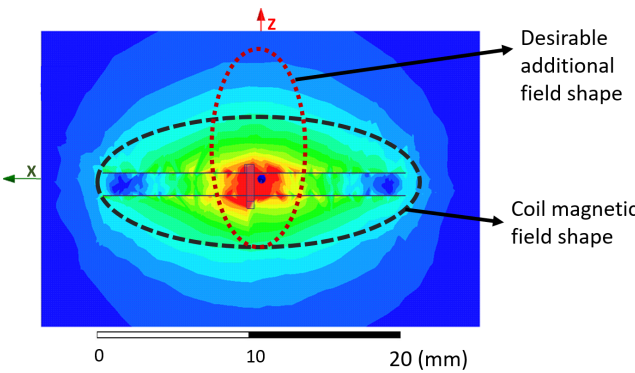


Fig. 3: Simulation of coil magnetic field intensity shape. The current generated magnetic field shape and an additional desirable shape have been outlined with dashed lines

IV. ENHANCEMENTS ON COIL BOARD

As previously discussed, the strength of the magnetic field generated by the Coil Board needs to be increased. There are several ways to accomplish this. One way is to expand the diameter of the flat coil in order to increase the number of loops in the coil. However, this solution would increase the overall footprint of the sensor, which is an unwanted result. Another solution would be increasing the number of loops of the coil into more layers of the PCB. Yet, this modification would make the PCB thicker, which is not wanted either.

Furthermore, the shape of the generated field needs to be considered. The magnetic sensor present different resolutions for X-Y axes and Z-axis (maximum reading values of $1.3mT$ for X-Y and $2.5mT$ for Z). Due to this characteristic, an homogeneous increase of the shape of the magnetic field would saturate X or Y axes before fully utilizing the available spectrum of Z-axis. Please refer to Fig. 3. The figure shows a simulation of the coil of the PV with $1500mA$ of current passing through it. The shape of the generated field intensity has been pointed out with a dashed black line. Increasing the number of loops of the coil would inflate the marked area of the elliptical shape, resulting in a rounder shape. Rather than a global increase of the magnetic field, an additional stronger vertical component would be beneficial to excite the Z-axis sensor in a greater proportion than X and Y axes (that offer lower sensing resolutions). The desired shape has been highlighted with a dashed red line in Fig. 3.

An idea to reach the desirable shape is to use a small permanent magnet at the center of the Coil Board. This solution would serve a double purpose of boosting the overall strength of the coil while also generating a focused central field by combining the effects of the electromagnet and small permanent magnet. Fig. 2 includes an arrow to the permanent magnet's location, at the center of the Coil Board of the NV.

To test this proposal, we selected two small neodymium cylindrical magnets: one with dimensions of $1.59 \times 0.53mm$ and a rating of N50 (from now on referred to as 'Big Magnet'), and another magnet with dimensions of $0.97 \times 0.51mm$ and rating of N35 (from now on referred to as 'Small

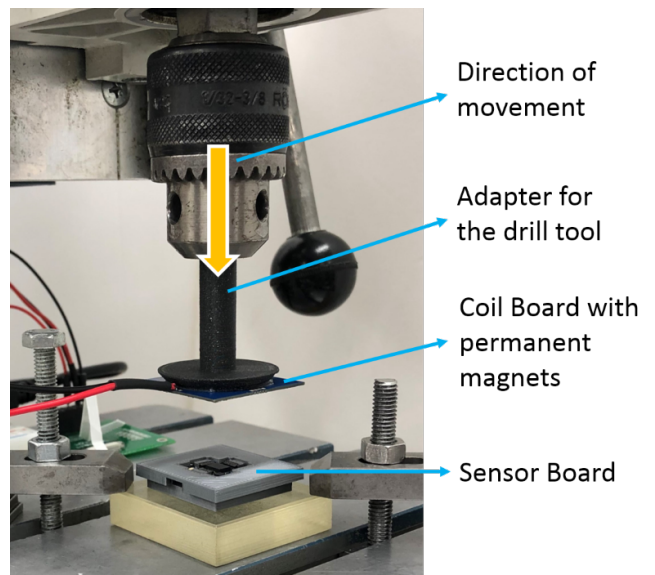


Fig. 4: Vertical approach setup to measure the magnetic field generated by the Coil Board and the added permanent magnets

Magnet').

Next, we ran simulations using ANSYS Maxwell software to check the following three different scenarios of permanent magnets attached to the center of the Coil Board:

- Case 1: one Big Magnet.
- Case 2: one Small Magnet.
- Case 3: two stacked Small Magnets.

The electromagnet was simulated with a direct current of $1500mA$ passing through it and then the three permanent magnet cases were situated directly on top of the coil. Fig. 5 shows the static simulation results with magnetic intensity on a logarithmic scale. We argue that the best case is Case 2 (one Small Magnet, picture in the middle of the composite figure) because the simulated shape best approaches the desired elliptical shape of Fig. 3, with a higher magnetic field intensity centered towards the vertical axis. The simulation of Case 2 shows an approximate oval shape with a magnitude of $2.0mT$ at a distance of $5mm$ from the magnet on the Z axis. From the simulations it seems that Case 1 and Case 3 present stronger fields that would likely saturate X or Y axes quickly, with ranges close to $10.0mT$ and $35.0mT$ respectively, at a distance of $5mm$ along the Z axis from the center of the magnets. Moreover, the high intensity of these last cases could also quickly saturate also the Z axis, which would be an unwanted effect.

To empirically test these interpretations, a follow-up experiment was performed for each of the three permanent magnet cases. For the experiment, the Sensor Board was mounted on the base of a vertical milling machine bench and the Coil Board was attached to the drill tool hole using an ABS 3D printed adapter. Fig. 4 shows a picture of this setup with references to each component. The three permanent magnets were tested on the same setup (Big Magnet, one Small Magnet and two stacked Small Magnets).

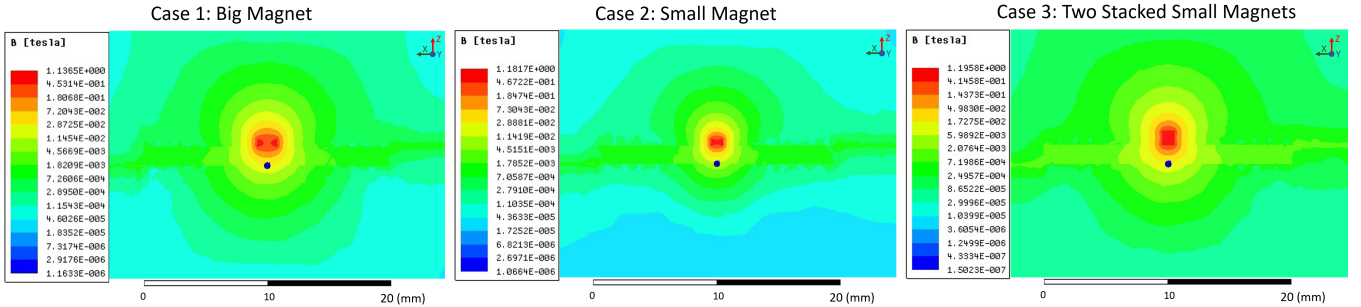


Fig. 5: Simulation results of Coil Board with permanent magnets

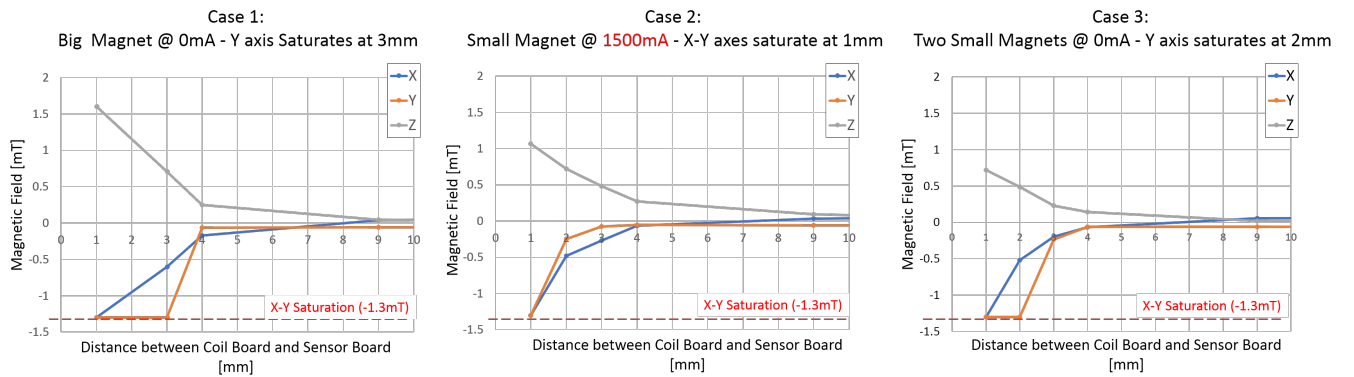


Fig. 6: Experiment results of Coil Board with permanent magnets. The preference for Case 2, is confirmed with best saturation points at a closer distance and higher coil current (1500mA)

The objective of the experiment was to check the strength of the hybrid arrangement of permanent magnet and coil-generated magnetic field under different values of direct current. Then we checked the *distance* and *current value* at which any of the magnetic sensors axes got saturated. Three different current values were used: *0mA* (no current on the coil, used to check the influence of the permanent magnet only), *750mA* (half of the maximum current value on coil) and *1500mA* (maximum current value).

While applying the different current values on the coil, the board was manually lowered at intervals, bringing the Coil Board closer to the Sensor Board. No material was placed between the two boards for this experiment. Each permanent magnet was manually fixed at the center of the Coil Board.

The results are condensed in three graphs, one for each of the permanent magnet cases. Only the saturation cases are presented. As predicted from the simulations, Cases 1 and 3 saturate the sensor faster than Case 2. Case 1 saturates the Sensor Board Y-axis at a distance of *3mm* with *0mA* (no current) applied to the coil. Case 2 starts to saturate both X and Y axes at a lower distance of *1mm* and, important to notice, at a coil current value of *1500mA* (maximum value). These results support the initial preference of Case 2, so this configuration of a single Small Magnet is adopted for the sensor module. Moreover, it should be noticed that in Case 2 the values for Z-axis have doubled from the values

of the coil without the permanent magnet. Now reaching a maximum of *1.2mT*, compared to the no-magnet version of *0.6mT* at *1500mA* current and *1mm* distance.

As a final comment regarding the early saturation of Y-axis, we suggest that this effect corresponds to the fact that there is no information available about the exact location of the magnetometer sensor inside the SoC of the BMF055 chip, so the coil and magnetometer sensor cannot be perfectly aligned. If they were, saturation should be seen for X and Y axes at the same point (distance and current).

V. ENHANCEMENTS ON MIDDLE LAYER

According to the presented results (Fig. 6), the distance range between the coil and sensor boards in which the magnetic field grows in an exponential fashion is $1mm < d < 5mm$. With a minimum of *1mm*, at which point some axes get saturated. From the previous version of the module it was noticed that the *3mm* open-cell polymer foam used as middle material did not yield good displacement values for either normal or shear forces. In particular, the maximum shear deformation that the PV material would allow was approximately *0.8mm*. We argue that this small deformation was partially due to the material characteristics, as open-cell polymers only allow comparatively small shear forces before reaching breaking point. Additionally, the thickness of the material also affects the maximum displacement it would allow before breaking; in this respect, a thicker material would be preferable. Finally, the overall thickness of the NV

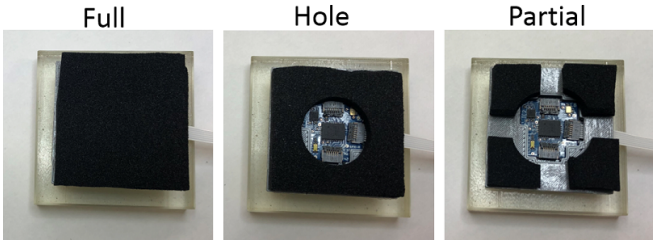


Fig. 7: Three cases of tested neoprene shapes

module should be maintained or reduced from the PV (which thickness was 8.2mm).

Therefore, we selected a 5mm neoprene material (from Matec Sozai) as Middle Layer. With this material, the overall thickness of the NV sensor is 7.2mm (Fig.1).

Once the new material had been selected, experiments were performed to test the response of different shapes for the Middle Layer. One more time, three possible shapes were selected as candidates. They will be called as follows: 'Full', 'Hole' and 'Partial'. 'Full' is a 30x30mm square shape, 'Hole' has the same outer shape with a 16mm diameter circle of removed material in the center and 'Partial' is four sections at the corners of the board. Please refer to Fig.7 for a visual reference of the shapes.

Sensor modules were assembled with each of these shapes and tested (the Coil Board with the Small Magnet just presented). The setup used in these experiments is presented in Fig.8. The base is a CTS150 X-Y table (from IKO) that can be programmed to move the sensor in the X-Y plane. Then a VMS05-180-LB voice coil motor (from H2W) is mounted vertically in series with a Nano17 6-axis force-torque sensor (from ATI). The Nano17 is mounted on the shaft of the voice coil motor, which is used to press with a known force onto the sensor module. All components of the setup and the sensor module being tested are operated by a single computer. In order to separate the sensor module from the influence of the strong magnets present in the voice coil and the X-Y table, some spacers where 3D printed in ABS plastic (marked with references in Fig.8). Used data collection speeds were set to be 10Hz for the sensor module and 100Hz for the 6-axis force-torque sensor, the current maximum possible frequencies for those components.

The three different neoprene shapes were tested on both Normal and Shear force with a current value of 1500mA applied to the Coil Board.

For the Normal force experiment, the voice coil pushed down on the sensor module with seven increasing steps of force reaching a maximum of $\approx 47N$.

For the Shear force experiment, the voice coil pushed down one time on the sensor to increase the friction between the 6-axis sensor and our prototype sensor. After this first small compression, the X-Y table was programmed to move in an oscillating fashion with steps, increasing the displacement distance from the center on every oscillation to a maximum of 3mm from the center of the sensor.

The results for both normal and shear force experiments

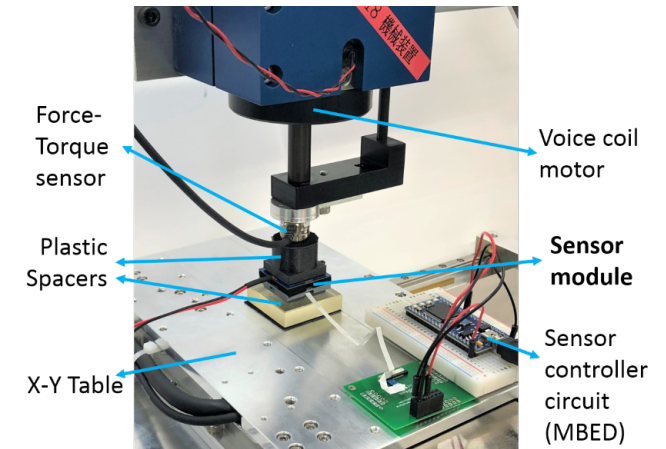


Fig. 8: Normal and shear force test setup

can be found in Fig. 9. All three different material shapes are shown, condensed into two graphs. From the graph on the right side, that shows the normal force reaction of the material shapes, it can be noticed that the 'Full' case shows the lowest variation in the measured Z axis. The 'Hole' case achieved slightly higher values than the 'Full'; however, the 'Partial' shape outperformed both previous cases. Similar results can be found in the graph on the left side, corresponding to shear force measurements. From these results, it is clear that the 'Partial' shape is the one that offers higher deformations for the same forces applied to the sensor. This is convenient because it utilizes the broadest bandwidth of the available sensing spectrum, which was one of the main motivations for this work. Furthermore, higher deformation values correspond to a more compliant sensor where small differences of applied forces would be easier to detect and classify. Therefore, the 'Partial' shape will be selected for further iterations of the sensor module. Calibration procedures and further sensor characterization will be explored in future works.

VI. CONCLUSIONS & FUTURE WORKS

An enhanced version of our sensor module has been presented. The problematic area relating to the weakness and shape of the generated magnetic field of the coil has been addressed by adding a small permanent magnet to the center of the board. Three different magnet arrangements were tested and a single magnet measuring 0.97x0.51mm and with rating of N35 was selected as optimal. This addition provides an increased and focused effect in the overall magnetic field without saturating any axes of the sensor. The first version of the sensor used a Coil Board that generated 0.25mT of maximum magnetic field intensity at 1mm vertical axis distance from the board; the new version with a new Coil Board and an added permanent magnet generates 1.2mT at the same point.

Furthermore, three different shapes of neoprene material were tested to act as Middle Layer of the sensor module. Results have shown that the most desirable shape correspond

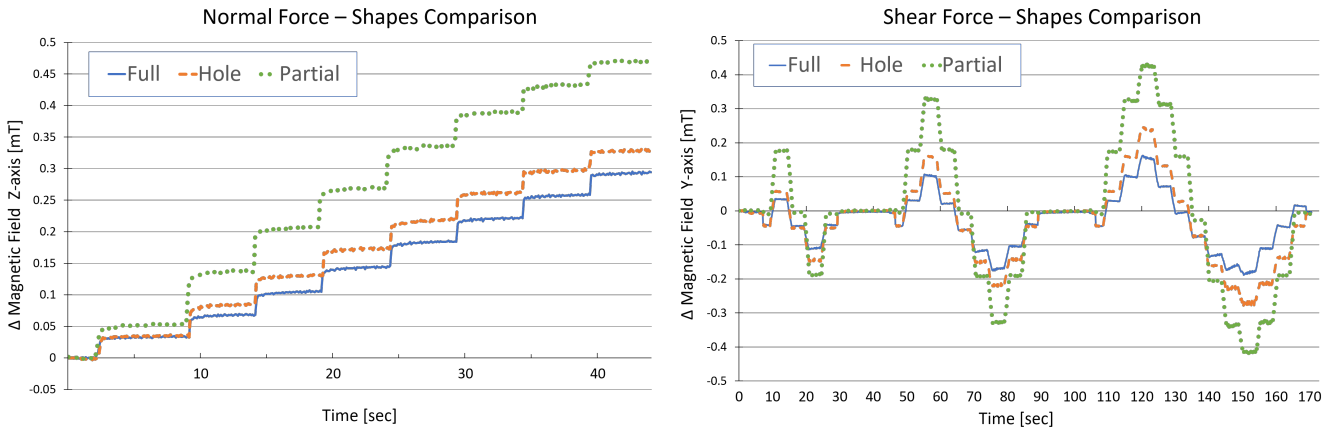


Fig. 9: Experiment results for three different neoprene shapes to be used as Middle Layer

to the 'Partial' shape, which is the one that covers the smallest area between the boards of the module. Experiment results have shown that this shape deforms more than the other investigated options, which in turn results in higher sensed values. The maximum deformation value of the sensor on the X-Y plane was found to be 0.8mm for the first version. In contrast, the current version with the new middle material, was tested at a maximum lateral deformation of 3mm .

Finally, with the new middle material design, the current version was tested with a maximum normal force of 47N while the previous version could only reach 4.5N for the same experiment.

Further sensor characterization, hysteresis response and software to interconnect sensor modules will be included in future works. Higher sensing speeds (than the current 10Hz) have to be considered and implemented. Finally, the adjustability of the Coil Board and its relation with the permanent magnet field will have to be investigated in detail to determine the limits of the sensor module.

ACKNOWLEDGMENT

This research was supported by the JSPS Grant-in-Aid for Young Scientists (B) No.17K18183 and (B) No. 19K14948 and the Grant-in-Aid for Scientific Research No.19H01130. Additional support was provided by the Ministry of Education, Science, Sports and Culture of Japan (Monbukagakusho).

REFERENCES

- [1] J. Wainer, D. J. Feil-Seifer, D. A. Shell, and M. J. Mataric, "Embodiment and human-robot interaction: A task-based perspective," in *RO-MAN 2007 - The 16th IEEE International Symposium on Robot and Human Interactive Communication*, pp. 872–877, Aug 2007.
- [2] I. Rae and L. Takayama, "In-body experiences : Embodiment , control , and trust in robot-mediated communication," vol. 15, 04 2013.
- [3] J. Ventre-Dominey, G. Gibert, M. Bosse-Platiere, A. Farnè, P. F. Dominey, and F. Pavani, "Embodiment into a robot increases its acceptability," in *Scientific Reports*, 2019.
- [4] C. Bartolozzi, L. Natale, F. Nori, and G. Metta, "Robots with a sense of touch," *Nature Materials*, vol. 15, pp. 921 EP –, Aug 2016.
- [5] R. S. Dahiya, G. Metta, M. Valle, and G. Sandini, "Tactile sensing from humans to humanoids," *IEEE Transactions on Robotics*, vol. 26, pp. 1–20, Feb 2010.
- [6] A. C. Holgado, J. A. Alvarez Lopez, A. Schmitz, T. Pradhono Tomo, S. Somlor, L. Jamone, and S. Sugano, "An adjustable force sensitive sensor with an electromagnet for a soft, distributed, digital 3-axis skin sensor," pp. 2582–2588, 10 2018.
- [7] T. P. Tomo, A. Schmitz, W. K. Wong, H. Kristanto, S. Somlor, J. Hwang, L. Jamone, and S. Sugano, "Covering a robot fingertip with uSkin: A soft electronic skin with distributed 3-axis force sensitive elements for robot hands," in *2017 IEEE/RSJ IROS*, IEEE, 2017.
- [8] H. Wang, G. de Boer, J. Kow, M. Ghajari, A. Alazmani, R. Hewson, and P. Culmer, "A low-cost soft tactile sensing array using 3d hall sensors," *Procedia Engineering*, vol. 168, pp. 650 – 653, 2016. Proceedings of the 30th anniversary Eurosensors Conference Eurosensors 2016, 4-7. September 2016, Budapest, Hungary.
- [9] P. Mittendorfer, E. Yoshida, and G. Cheng, "Realizing whole-body tactile interactions with a self-organizing, multi-modal artificial skin on a humanoid robot," *Advanced Robotics*, vol. 29, no. 1, pp. 51–67, 2015.
- [10] H. Wang, J. W. Kow, N. Raske, G. de Boer, M. Ghajari, R. Hewson, A. Alazmani, and P. Culmer, "Robust and high-performance soft inductive tactile sensors based on the eddy-current effect," *Sensors and Actuators A: Physical*, 2017.